

Hong-Ou-Mandel two-photon x-ray states

Liam T. Powers and Stephen M. Durbin*

Department of Physics & Astronomy, Purdue University, West Lafayette IN 47907-2036

(Dated: January 13, 2026)

We have observed Hong-Ou-Mandel interference of high-brightness synchrotron x-rays with a Mach-Zehnder interferometer, yielding two-photon states of potential interest for x-ray quantum optics.

The essence of single-photon states is perhaps best exemplified by Dirac's famous claim about Michelson interferometry that "Each photon then interferes only with itself. Interference with different photons can never occur" [1]. Parametric down-conversion (PDC) has since enabled the reliable generation of pairs of photons and interference involving two photons was reported by Hong, Ou, and Mandel (HOM) [2]. Two indistinguishable photons at separate entrance ports of a beam splitter generate two-photon interference, with destructive interference preventing the two photons from taking different exit paths. The Dirac claim was later updated to clarify that two-photon (or multi-photon) states only interfere with themselves. [3, 4]. Multi-photon states are now part of various quantum applications, including teleportation, optical computing, and quantum metrology [5–7].

Analogous progress with x-ray photons has been quite limited. Nearly all x-ray science is still in the Dirac single-photon-interference phase despite the enormous advances at synchrotron and free electron laser sources [8]. The exceptions include Hanbury Brown - Twiss observations and x-ray parametric down-conversion [9–14].

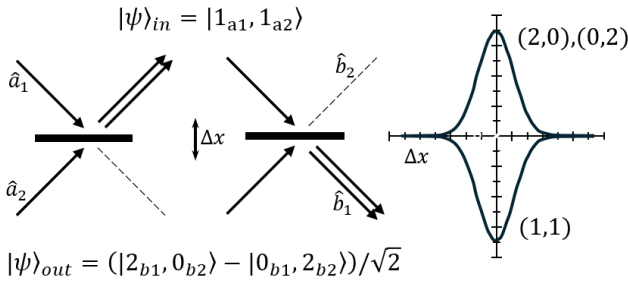


FIG. 1. Hong–Ou–Mandel (HOM) interference. Left: A 50-50 beam splitter with indistinguishable incident photons produces either two photons exiting from one output port or two photons exiting from the other. The output wavefunction $|\psi\rangle_{\text{out}}$ is a coherent superposition of these two configurations. Right: Idealized plot of the coincidence rate for one photon exiting each output port, $(1, 1)$, as a function of beam-splitter displacement Δx , showing the HOM dip. Also shown is the corresponding peak in the rate of two photons exiting from the same port, $(2, 0)$ and $(0, 2)$.

We report observation of two-photon interference with x-rays. Since this produces maximally entangled N00N states ($N=2$), this first step could lead to the use of entangled x-rays as a practical quantum probe as well as other multi-photon applications [15].

Two-photon interference with a synchrotron source has these requirements: the source generates pairs of indistinguishable photons, these pairs are split to take separate paths, a scanning beamsplitter varies their spatial and temporal overlap to sample the region where their diffracted outputs are indistinguishable, and a multi-photon counting detection system counts the number of photons in each exit beam for each synchrotron pulse.

A synchrotron source contains many modes for each wavelength λ , and the occupation of these modes is described in terms of the peak brightness B :

$$n_{\text{ph}} = \frac{B \lambda^3}{4\sqrt{2}c} \quad (1)$$

where c is the speed of light [16]. At high-brightness synchrotrons such as the APS-U at Argonne National Lab, where this work was conducted, this photon occupation factor can now be greater than unity for certain energies. Assuming a thermal distribution the probability of k photons being found in a given mode is [17]

$$P_k = \frac{n_{\text{ph}}^k}{(1 + n_{\text{ph}})^{k+1}} \quad (2)$$

For example, at $n_{\text{ph}} = 2$ more than 22% of photons are born in a doubly occupied mode, but there is a significant background from other modes for a given pulse. Interference measurements should be possible over a range of occupation values, depending on sensitivity to signal-to-background ratio.

To achieve interference, the synchrotron beam is monochromated to a specified energy E and bandwidth ΔE , as indicated by the high heat-load and high energy-resolution monochromators shown in Figure 2(a). Pairs of photons can be split by the initial beamsplitter and redirected by the Bragg mirrors of a specially constructed Mach-Zehnder interferometer using Si [400] reflections. The two beams are recombined at the final beamsplitter where interference can occur. Each beamsplitter is a thin Si crystal set to diffract in the Bragg geometry. Figure 2(b) shows rocking curve intensities at both detectors for the final beamsplitter over a narrow angular

* durbin@purdue.edu

range when both beams intersect and simultaneously satisfy the Bragg condition. In the wings of the rocking curve, the splitter is essentially transparent, but in the center each beam is equally reflected and transmitted at a precise angular position, satisfying the requirement for a 50–50 beamsplitter [18].

Both splitters are controlled by precision linear and rotary stages, critical for ensuring that all elements are diffracting optimally and the two equal-length beam paths intersect at the second beamsplitter. Overlap was calibrated with an x-ray fluorescent powder coating on the beamsplitter and observing beam spots with a camera, and confirmed by rocking curve measurements (Fig 2). Following the original HOM protocol (Fig 1), the beamsplitter is translated by fixed values of Δx to vary the overlap of the two beams.

To minimize background contributions and prevent detector saturation, it is ideal to have an average of two incident photons per synchrotron pulse. Taking values from Table 1, the full beam would yield about 10^5 photons per pulse, a number that is already reduced due to a

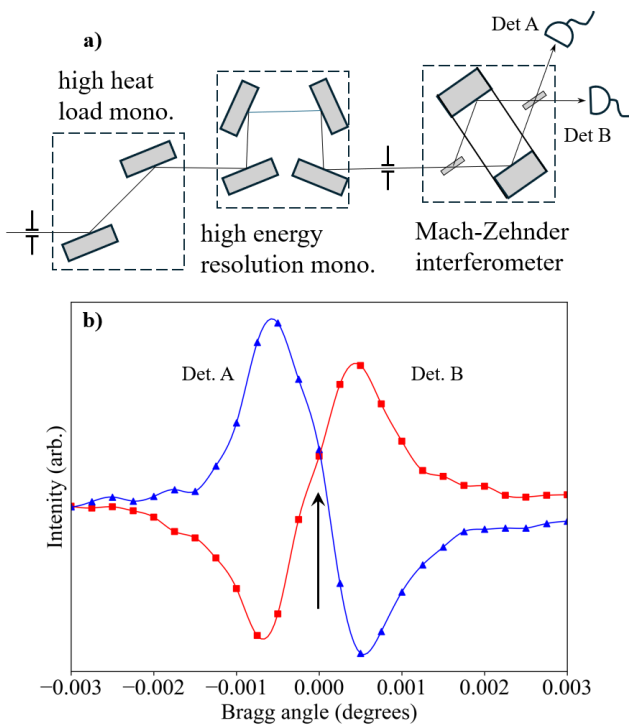


FIG. 2. Schematic of beamline optics. (a) Synchrotron radiation enters from the left through the white-beam slits and is monochromated by a high heat-load monochromator. That exit beam enters the high energy-resolution monochromator to reduce the band width. After another set of slits, the beam enters the Mach-Zehnder interferometer; the final splitter is where HOM interference can occur. Exit beams are detected by dual APDs. (b) HOM beamsplitter rocking curves for both detectors versus angular shift; arrow denotes location where each incident beam is equally reflected and transmitted.

relatively small monochromator band width. The needed reduction is obtained primarily by reducing the beam size with slits, which in principle preserves brightness.

An ideal interference measurement requires counting the integer number of photons at both detectors from each synchrotron pulse. The voltage outputs of photon-number-resolving avalanche photodiode (APD) detectors are digitized and analyzed by a fast FPGA system and stored before the next pulse arrives [19]. This permitted the independent analysis of 13 million discrete events per second (i.e. the synchrotron pulse frequency), a new experimental modality where each pulse is a unique measurement. Each output signal is converted to an integer number of photons (0, 1, 2...) based on prior calibration (Fig 3(a,b)).

Figure 3 presents the results of a representative dataset in which the numbers of coincident (1, 1) pairs and of (2, 0), (0, 2) pairs collected during 10 seconds of beam exposure were recorded as a function of beam-splitter displacement Δx . A HOM dip is apparent in the total (1, 1) count, accompanied by a corresponding peak in the number of (2, 0), (0, 2) pairs. For an incident flux of 1.63×10^6 Hz in the (1, 1) channel, about 3×10^4 Hz are suppressed at the dip minimum and converted into an

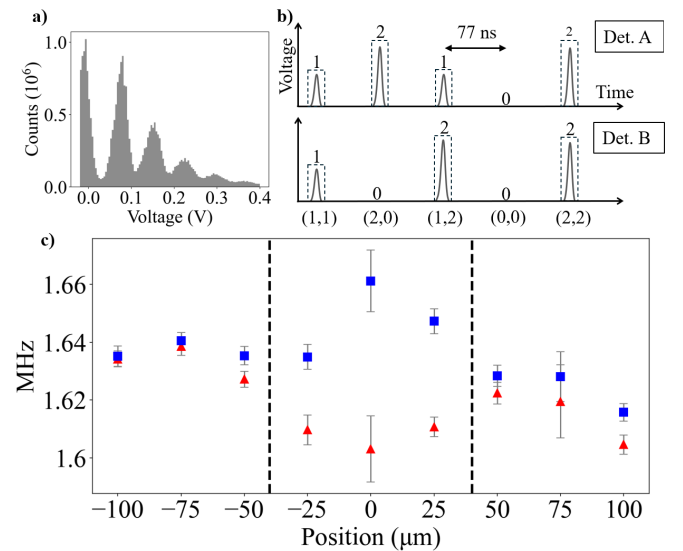


FIG. 3. Raw count-rate data. (a) Histogram of avalanche photodiode (APD) detector output from 13 MHz synchrotron x-ray pulses; mean count per pulse is approximately unity. (b) After conversion of the APD outputs to integer values, each synchrotron pulse is represented by a pair of integers, e.g., (1, 1), (2, 0), or (0, 2). (c) Measured rates of (1, 1) pairs and of (2, 0), (0, 2) pairs as a function of beam-splitter displacement Δx , revealing a Hong–Ou–Mandel dip in the (1, 1) rate and a corresponding peak in the two-photon rate. Each data point is the average of five scans of 2 s duration, converted to units of Hz. A baseline shift of $+0.1 \times 10^6$ Hz has been applied to the raw (1, 1) data to facilitate comparison. The marker indicates the range of overlap between the beam splitter and the intersecting $\sim 80 \times 80 \mu\text{m}^2$ beams.

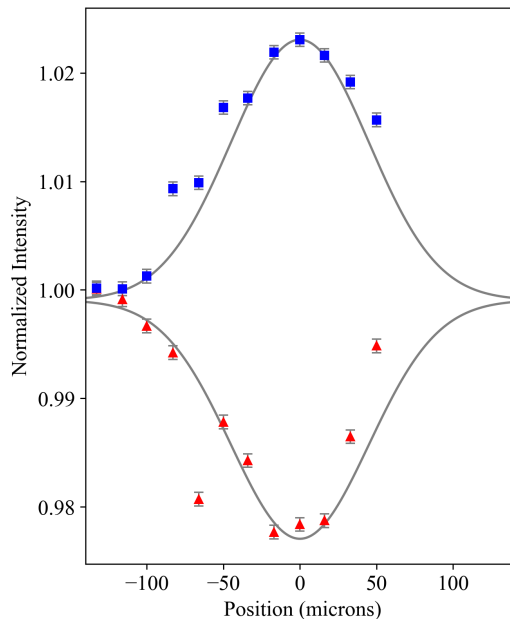


FIG. 4. HOM interference. The (1, 1) and the (2, 0) & (0, 2) rates are plotted versus beamsplitter position Δx , revealing the HOM dip and peak.

equal number of (2, 0), (0, 2) pairs. This constitutes clear evidence that pairs of indistinguishable photons emerge from the beam splitter as two-photon x-ray states.

Results from a separate beamtime are shown in Figure 4, where a comparable dip is observed. These data are normalized to off-interference coincidence flux rates which equals unity in the wings. The similarity of data sets in Figures 3 & 4 establishes the repeatability of this technique between beamtimes.

To determine the mode occupation factor n_{ph} , we note that Eqn. 2 gives $P_2/P_1 \approx n_{ph}$ when this factor is much less than unity. For P_2 we double the observed dip of 3×10^4 pairs/s since only half of incident pairs take dif-

TABLE I. Synchrotron parameters

Parameter	Notation	Value	Units
Photon energy	E	8.0	keV
Photon wavelength	λ	1.5	Å
Energy resolution	ΔE	74	meV
Bunch frequency	f	13.0	MHz
Stored current	I	130	mA
Source size, horizontal ^a	σ_h	28	μm (FWHM)
Source size, vertical ^a	σ_v	19	μm (FWHM)
Lateral coherence width (hor.) ^b	l_h	93	μm
Lateral coherence width (vert.) ^b	l_v	140	μm
Longitudinal coherence length ^b	l_{long}	8	μm
Source distance	R	35	m
Bunch duration	τ	230	ps (FWHM)

^a See Ref. [20]

^b $l_{h,v} = \frac{1}{2}\lambda R/\sigma_{h,v}$ and $l_{long} = \frac{1}{2}\lambda E/\Delta E$ [21].

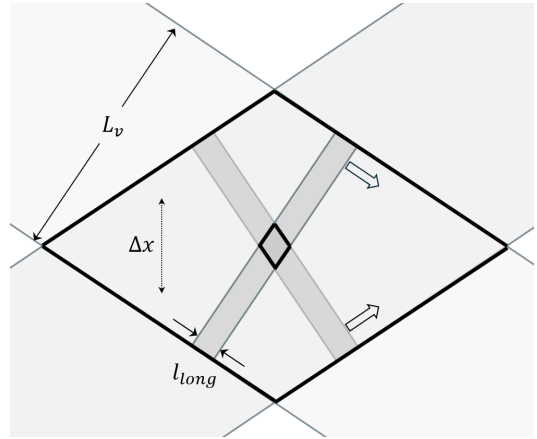


FIG. 5. Intersection of overlapping x-ray beams. A HOM dip is observed when the beamsplitter samples the large diamond, where beam width L_v is set by the vertical slit and is smaller than the lateral coherence length; Δx indicates the direction of beamsplitter displacement. The smaller diamond is the overlap of the longitudinal coherence length of two simultaneous x-rays. Interference occurs even when the beamsplitter is outside this diamond, where the photons never overlap temporally.

TABLE II. Brightness calculations

Quantity	Notation, units	Full beam	HOM beam
Photons per second	I , ph/s	1.3×10^{12}	2.6×10^7
Hor. slit \times vert. slit	$L_h \times L_v$, mm ²	1×1	0.08×0.08
Solid angle	Ω , mrad ²	8.1×10^{-4}	5.2×10^{-6}
Source size (rms)	$\sigma_h \sigma_v$, mm ²	9.6×10^{-5}	9.6×10^{-5}
Bandwidth	$\Delta E/E$ (0.1%)	9.2×10^{-3}	9.2×10^{-3}
Brightness (avg) ^b	B_{avg}	1.8×10^{21}	5.6×10^{18}
Peak brightness ^{b,c}	B_{peak}	6.0×10^{23}	1.8×10^{21}
Photon degeneracy ^d	n_{ph}	1.2	4×10^{-3}

^b Standard units ph/s/mrad²/mm²/0.1% bandwidth

^c Corrected for the duty cycle τf .

^d Eq. (1).

ferent paths through the interferometer. For P_1 we substitute the total photon rate of 26 MHz, which yields $n_{ph} \approx 0.002$. This can be compared to the occupation factor determined from the beam brightness (Eqn. 1). We first find the brightness of the full beam in front of the interferometer, using the nominal values of the synchrotron source size, the angles subtended by the beam slits, and the number of photons per second [20]. This yields an average brightness of 1.8×10^{21} in standard units and a photon occupation factor of 1.2, ample for HOM interference. (All parameters are given in Table II.) The same calculation after the Mach-Zehnder interferometer, however, reveals a large drop of only 5.6×10^{18} and a mean occupancy of $n_{ph} = 0.004$, in good agreement with the measured HOM dip result.

While some losses are expected from air absorption and the dispersion mismatch between the monochromators and the interferometer, the significant drop in brightness

caused by inserting slits to intercept a small fraction of the incident beam suggests an unexpected divergence of the x-rays. This is due to imperfect diffraction from the first crystal of the high heat load monochromator. This hypothesis is supported by observed changes to the beam profile when the upstream white beam slits were used to reduce the heat load on the element. Future measurements with full brightness should reveal much stronger HOM interference.

The original HOM dip determined the single-photon coherence time, but our result depends instead on the beam width. Figure 5 shows the relative size of the intersection of the two full beams of width $L_V \sim 80 \mu\text{m}$ compared to the temporal overlap of photons with longitudinal widths $l_{long} \sim 8 \mu\text{m}$, to scale. Note that interference is observed even when the beamsplitter samples regions outside the region of temporal overlap, showing that two-photon interference does not require simultaneous arrival at the same position on the beamsplitter. This effect has been addressed previously [3, 22–24]. That HOM only observed simultaneous photons shows that their spatial overlap (the large diamond in Fig. 5) was comparable to the temporal overlap (small diamond).

Finally, we note that these HOM-generated two-photon states sit on top of a significant background of single-photon states. There have been several experimental observations of optical two-photon states diffracting from slits with a wavelength $\lambda/2$ despite the single-photon wavelength λ [7, 25–27]. It has been suggested

that it should be possible to observe a similar effect with crystal diffraction [28]. If the exit beams containing two-photon states are made to diffract from a crystal such that $\lambda/2$ states will diffract but λ diffraction is forbidden, it should be possible to remove the single-photon background from the two-photon signal. This would also allow the use of the full two-photon content of the synchrotron beam, a potential increase of up to a factor of 10^5 . If successful, pure beams of maximally entangled x-ray N00N states ($N = 2$) could be generated that would be useful probes for entangled materials.

ACKNOWLEDGMENTS

The experiments at APS-U Sector 27 (Argonne) benefitted enormously from the efforts of Diego Casa, Jung Ho Kim, and Thomas Gog. We also acknowledge valuable contributions at Purdue from Aidan Jacobsen and Madeline Kwasniewski. This research was supported by the U.S. Department of Energy through Contract No. DE-SC0023176 and was performed using beam time awarded at the Advanced Photon Source under DOI 10.46936/APS-191314/60015045. The Advanced Photon Source is a U.S. Department of Energy (DOE) Office of Science user facility operated for the DOE Office of Science by Argonne National Laboratory under Contract No. DE-AC02-06CH11357.

[1] P. A. M. Dirac, *The Principles of Quantum Mechanics* (Clarendon Press, Oxford, 1930).

[2] C. K. Hong, Z. Y. Ou, and L. Mandel, Measurement of subpicosecond time intervals between two photons by interference, *Phys. Rev. Lett.* **59**, 2044 (1987).

[3] Y.-H. Kim, Two-photon interference without bunching two photons, *Phys. Lett. A* **315**, 352 (2003).

[4] Z. Y. Ou, *Multi-Photon Quantum Interference* (Springer, Boston, 2007).

[5] D. e. Bouwmeester, Experimental quantum teleportation, *Nature* **390**, 575 (1997).

[6] P. e. Kok, Linear optical quantum computing with photonic qubits, *Rev. Mod. Phys.* **79**, 135 (2007).

[7] A. N. e. Boto, Quantum interferometric optical lithography: Exploiting entanglement to beat the diffraction limit, *Phys. Rev. Lett.* **85**, 2733 (2000).

[8] J. Stöhr, Overcoming the diffraction limit by multiphoton interference: A tutorial, *Adv. Opt. Photon.* **11**, 215 (2019).

[9] I. Freund and B. F. Levine, Parametric conversion of x rays, *Phys. Rev. Lett.* **23**, 854 (1969).

[10] N. J. e. Hartley, X-ray parametric down-conversion at an xfel, *Optica* **12**, 961 (2025).

[11] E. Gluskin, E. E. Alp, I. McNulty, W. Sturhahn, and J. Sutter, A classical hanbury brown–twiss experiment with hard x rays, *J. Synchrotron Rad.* **6**, 1065 (1999).

[12] O. Y. e. Gorobtsov, Diffraction-based hanbury brown–twiss interferometry at a hard x-ray free-electron laser, *Sci. Rep.* **8**, 2219 (2018).

[13] A. e. Singer, Hanbury brown–twiss interferometry at a free-electron laser, *Phys. Rev. Lett.* **111**, 034802 (2013).

[14] A. e. Singer, Intensity interferometry of single x-ray pulses from a synchrotron storage ring, *Phys. Rev. Lett.* **113**, 064801 (2014).

[15] J. P. Dowling, Quantum optical metrology—the lowdown on high-n00n states, *Contemp. Phys.* **49**, 125 (2008).

[16] J. Stöhr, Two-photon x-ray diffraction, *Phys. Rev. Lett.* **118**, 024801 (2017).

[17] R. Loudon, *The Quantum Theory of Light*, 3rd ed. (Oxford University Press, Oxford, 2000).

[18] L. T. Powers, M. Z. Kwasniewski, and S. M. Durbin, Variable bragg x-ray beam splitters, *AIP Adv.* **15**, 045231 (2025).

[19] L. T. Powers, A. M. Jacobsen, and S. M. Durbin, Counting multiple x rays per pulse with an avalanche photodiode detector, *J. Synchrotron Rad.* **32**, 629 (2025).

[20] X. e. Shi, Measurements of source emittance and beam coherence properties of the upgraded advanced photon source, *J. Synchrotron Rad.* **32**, 1152 (2025).

[21] J. Als-Nielsen and D. McMorrow, *Elements of Modern X-Ray Physics*, 2nd ed. (Wiley, Chichester, 2011).

[22] Y.-H. Kim, M. V. Chekhova, S. P. Kulik, and Y. Shih, Quantum interference by two temporally distinguishable pulses, *Phys. Rev. A* **60**, R37 (1999).

[23] Y. H. Kim and W. P. Grice, Quantum interference with distinguishable photons through indistinguishable path-

ways, *J. Opt. Soc. Am. B* **22**, 493 (2005).

[24] Y.-H. Kim, O. T. Slattery, P. S. Kuo, and X. Tang, Conditions for two-photon interference with coherent pulses, *Phys. Rev. A* **87**, 063843 (2013).

[25] H. Kim, O. Kwon, W. Kim, and T. Kim, Spatial two-photon interference in a hong-ou-mandel interferometer, *Phys. Rev. A* **73**, 023820 (2006).

[26] M. D'Angelo, M. V. Chekhova, and Y. Shih, Two-photon diffraction and quantum lithography, *Phys. Rev. Lett.* **87**, 013602 (2001).

[27] B. e. Dopfer, Brillouin scattering and dynamical diffraction of entangled photon pairs, *Phys. Rev. A* **52**, R2531 (1995).

[28] S. M. Durbin, Proposal for entangled x-ray beams, *J. Appl. Phys.* **131**, 224401 (2022).